Supplement of Atmos. Chem. Phys., 23, 2421–2437, 2023
https://doi.org/10.5194/acp-23-2421-2023-supplement

Atmospheric Chemistry and Physics
Open Access
EGU

Supplement of

The impacts of dust aerosol and convective available potential energy on precipitation vertical structure in southeastern China as seen from multi-source observations

Hongxia Zhu et al.

Correspondence to: Rui Li (rli7@ustc.edu.cn)

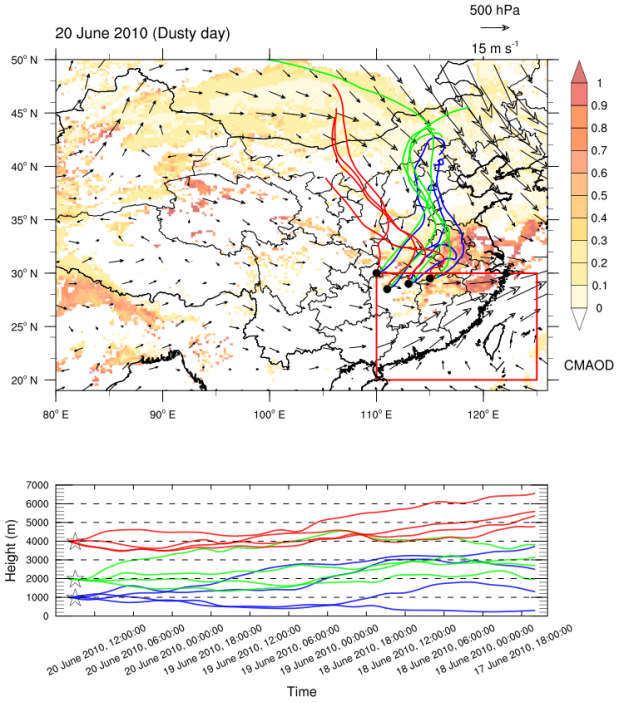

Figure S1: The horizontal distribution of coarse-mode aerosol optical depth derived from Terra MODIS, wind fields at 500 hPa, and 72 h back trajectories from the HYSPLIT model on 20 June 2010. The red box indicates the study area, and the geolocations of the four starting points are at 28.5° N, 111° E; 29° N, 113° E; 30° N, 110° E; and 29.5° N, 115° E, with altitudes of 1000 m (blue line), 2000 m (green line), and 4000 m (red line), extrapolated from 20 June 2010 at 13:00 UTC.

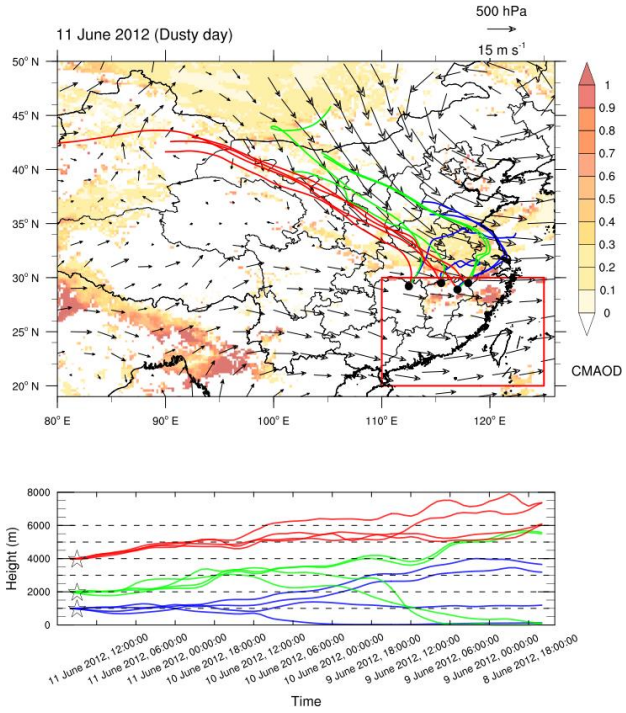

Figure S2: The horizontal distribution of coarse-mode aerosol optical depth derived from Terra MODIS, wind fields at 500 hPa, and 72 h back trajectories from the HYSPLIT model on 11 June 2012. The red box indicates the study area, and the geolocations of the four starting points are at 29.5° N, 115.5° E; 28.9° N, 117° E; 29.2° N, 112.5° E; and 29.5° N, 118° E, with altitudes of 1000 m (blue line), 2000 m (green line), and 4000 m (red line), extrapolated from 11 June 2012 at 18:00 UTC.

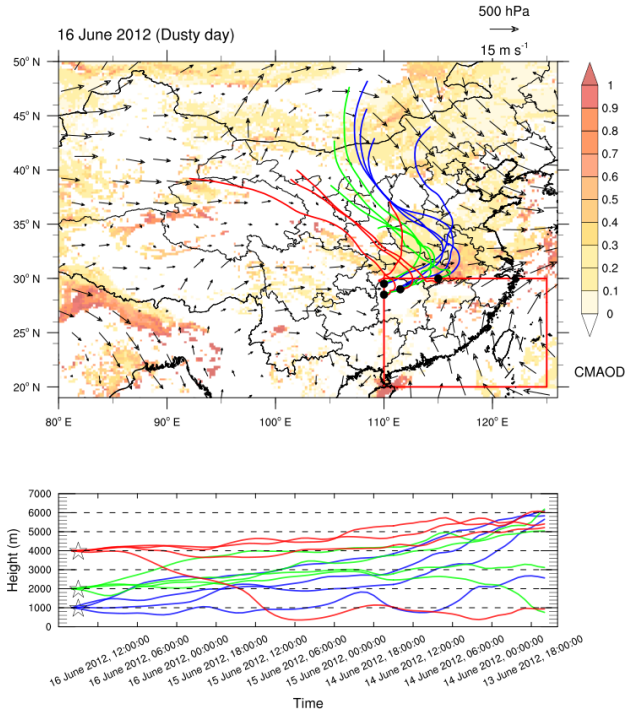

Figure S3: The horizontal distribution of coarse-mode aerosol optical depth derived from Terra MODIS, wind fields at 500 hPa, and 72 h back trajectories from the HYSPLIT model on 16 June 2012. The red box indicates the study area, and the geolocations of the four starting points are at 29.5° N, 110° E; 29° N, 111.5° E; 30° N, 115° E; and 28.5° N, 110° E, with altitudes of 1000 m (blue line), 2000 m (green line), and 4000 m (red line), extrapolated from 16 June 2012 at 13:00 UTC.

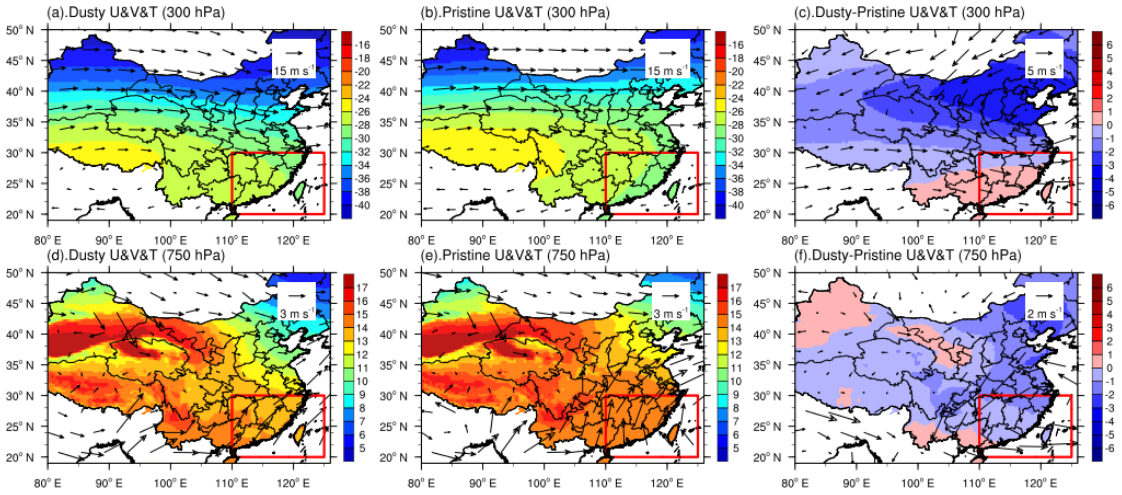

Figure S4: The fields of wind and temperature at 300 hPa (a,b) and 750 hPa (d,e) averaged from 46 selected dusty days (left column) and 92 selected pristine days (middle column) in JJA during the 2000-2013 period, based on ERA5 reanalysis data at a 0.25° × 0.25° horizontal resolution, and the associated differences between the two conditions for each variable (dusty minus pristine, right column).

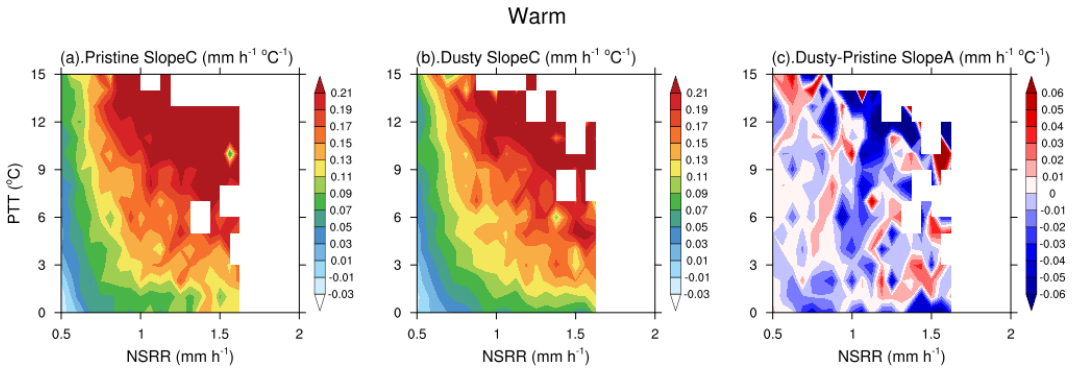

Figure S5: The mean SlopeC for warm rain as functions of near surface rain rate (NSRR) and precipitation top temperature (PTT) under pristine (the left column) conditions, dusty (the middle column) conditions and the differences between them (dusty minus pristine, the right column).

45

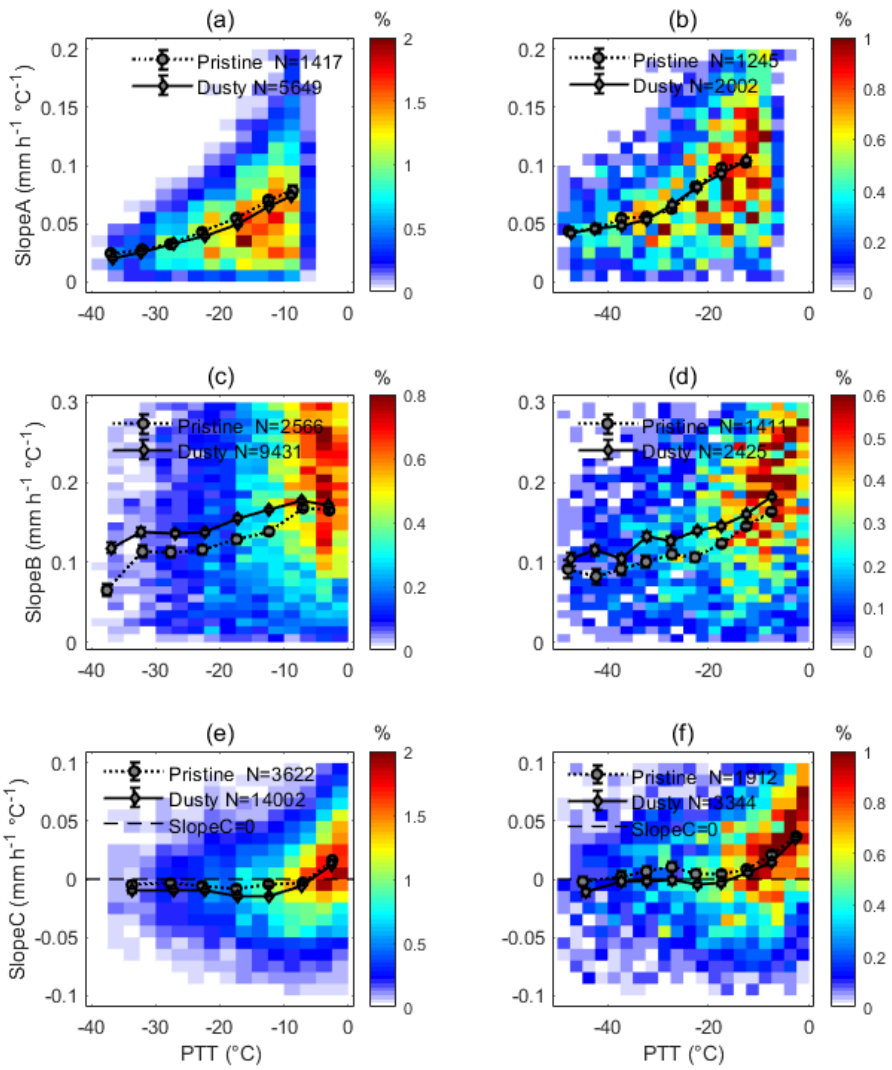

Figure S6: The mean SlopeA (a, b), SlopeB (c, d) and SlopeC (e, f) as functions of precipitation top temperature (PTT) for stratiform (the first column) and convective (the second column) rains under pristine (dotted line) and dusty (solid line) conditions. Overlapped are the contoured occur frequency (%) of samples under dusty conditions.

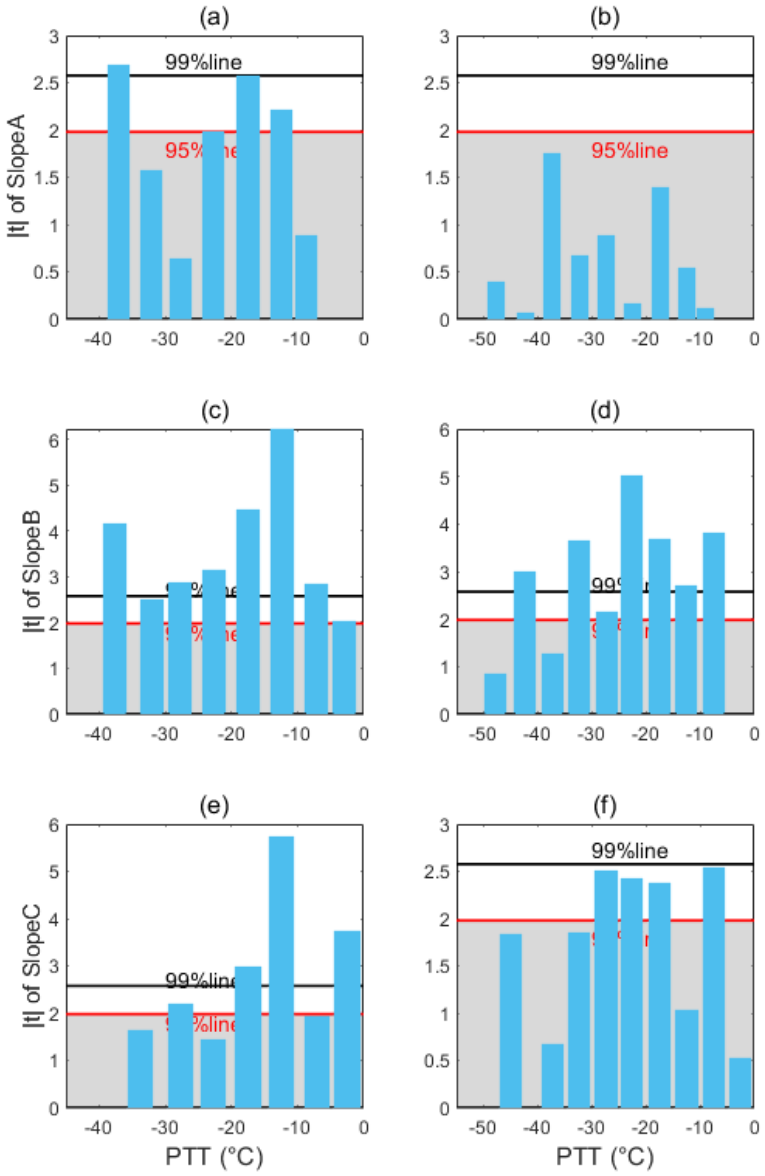

Figure S7: For a given PTT, t test significance for the differences between SlopeA (a, b), SlopeB (c, d), and SlopeC (e, f) of stratiform (the first column) and convective (the second column) precipitation for pristine and dusty conditions (red (black) line indicates the 95 % (99 %) confidence level at 100 degrees of freedom).

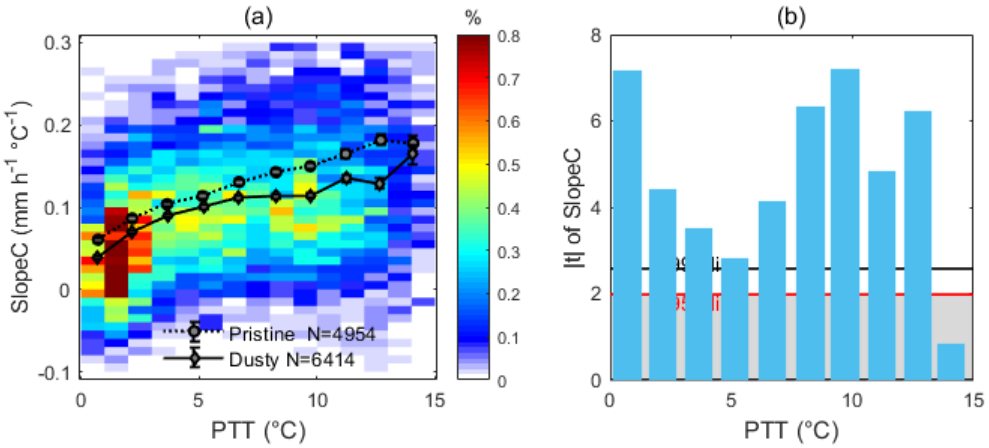

Figure S8: The mean SlopeC as functions of precipitation top temperature (PTT) for warm rain under pristine (dotted line) and dusty (solid line) conditions (a). Overlapped are the contoured occur frequency (%) of samples under dusty conditions. For a given PTT, t test significance for the differences between SlopeC of warm rain for pristine and dusty conditions (b), red (black) line indicates the 95 % (99 %) confidence level at 100 degrees of freedom.

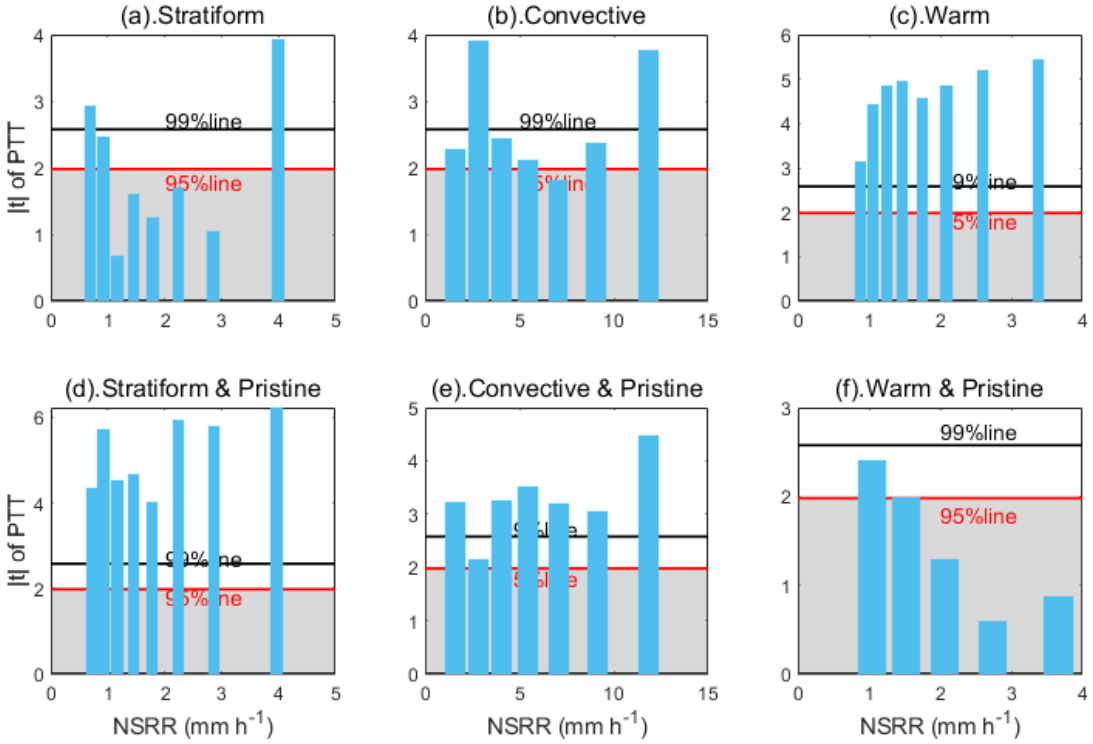

Figure S9: For a given NSRR, t test significance for differences in PTT between stratiform (a, d), convective (b, e) and warm (c, f) precipitation in pristine and dusty conditions (the first row) and between strong CAPE and weak CAPE in pristine conditions (the second row), red (black) line indicates the 95 % (99 %) confidence level at 100 degrees of freedom.

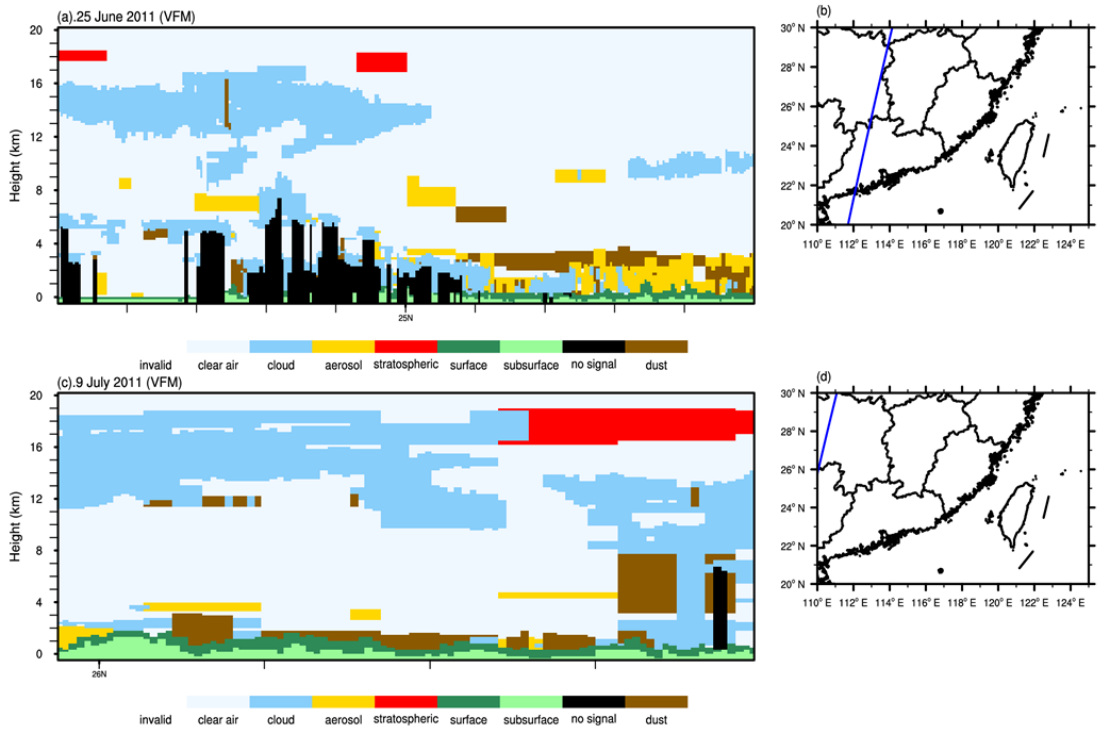

70

Figure S10: On June 25, 2011 and July 9, 2011, the vertical and horizontal distribution of cloud and aerosol layers observed by the Cloud-Aerosol Lidar and Infrared Pathfinder Satellite Observations (CALIPSO) lidar vertical feature mask (VFM) data product. Where the blue line in indicates the CALIPSO footprint.

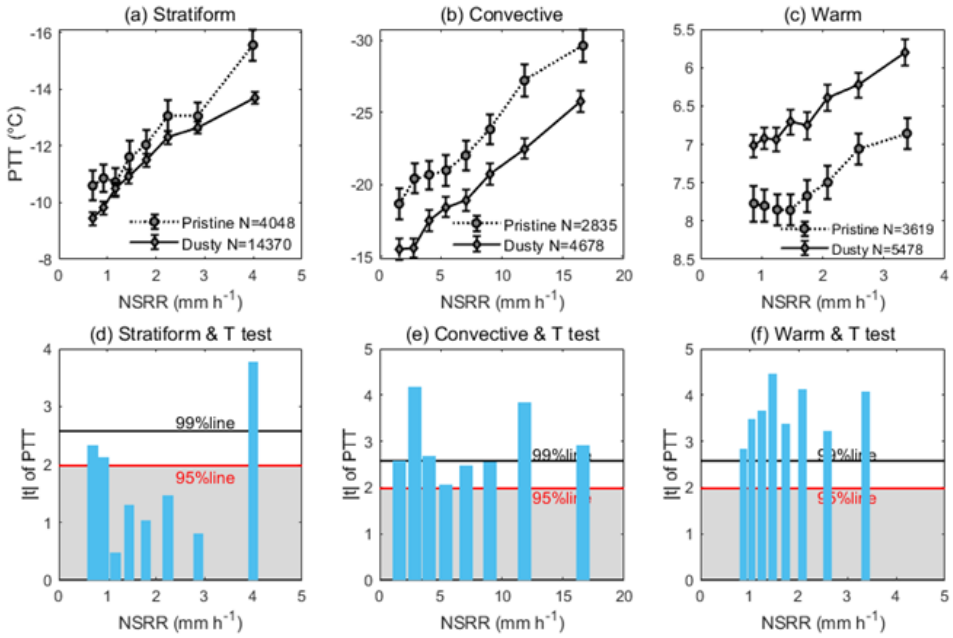

Figure S11: The precipitation top temperature (PTT) against near surface rain rate (NSRR) for new stratiform (a) , convective (b) and warm (c) precipitation samples under pristine (dotted curves) and dusty (solid curves) conditions (the first row). For a given NSRR, t test significance for differences in PTT between stratiform (d), convective (e) and warm (f) precipitation in pristine and dusty conditions (the second row), red (black) line indicates the 95 % (99 %) confidence level at 100 degrees of freedom.

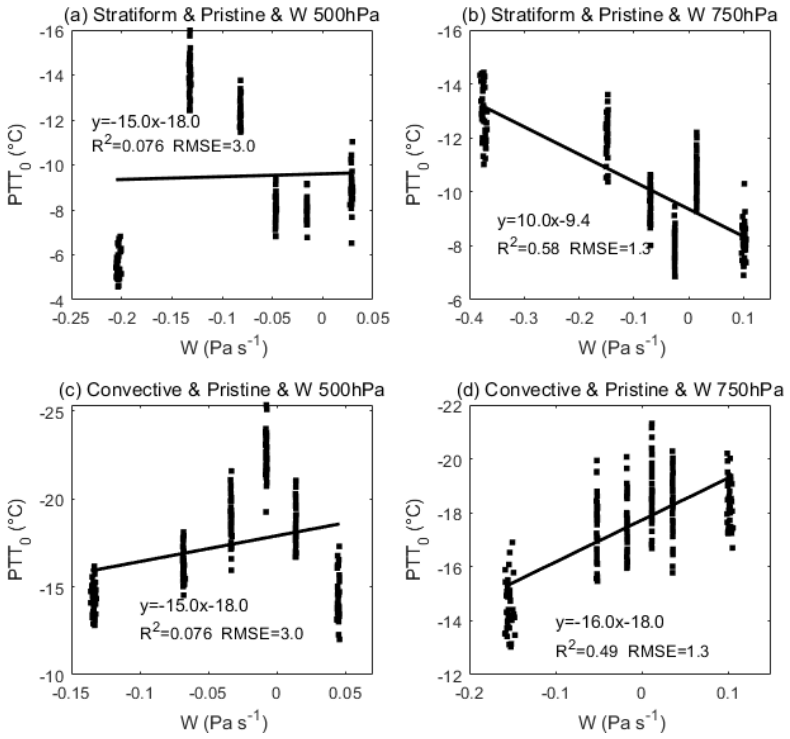

Figure S12: The variation of PTT_0 with updraft velocity (W, Pa s^{-1}) at 500 hPa (a,c) and 750 hPa (b,d) for deep stratiform precipitation (the first row) and deep convective precipitation (the second row) under pristine conditions. The results are derived from randomly selected 70% precipitation samples from total.

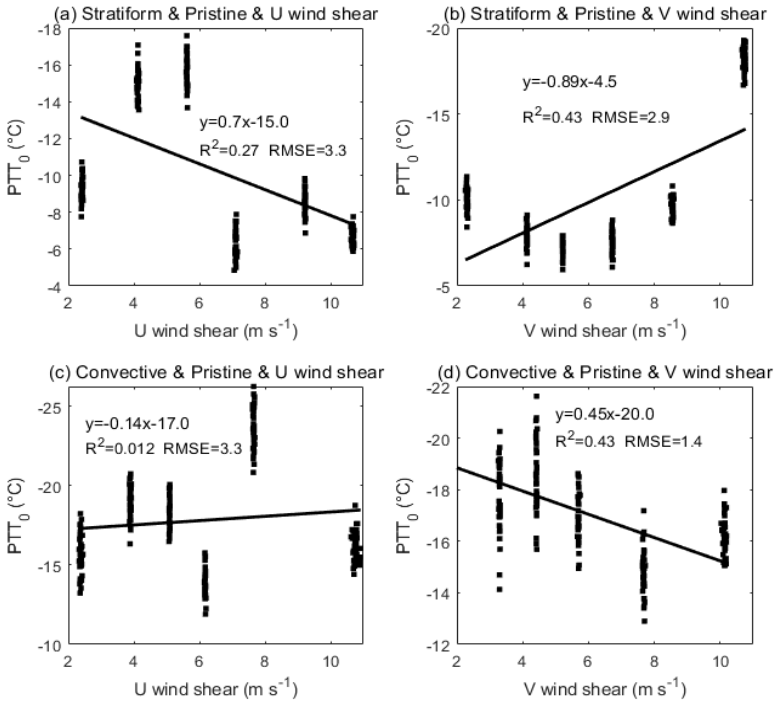

Figure S13: As same as Figure S12, but for U and V wind shear (m s^{-1}).

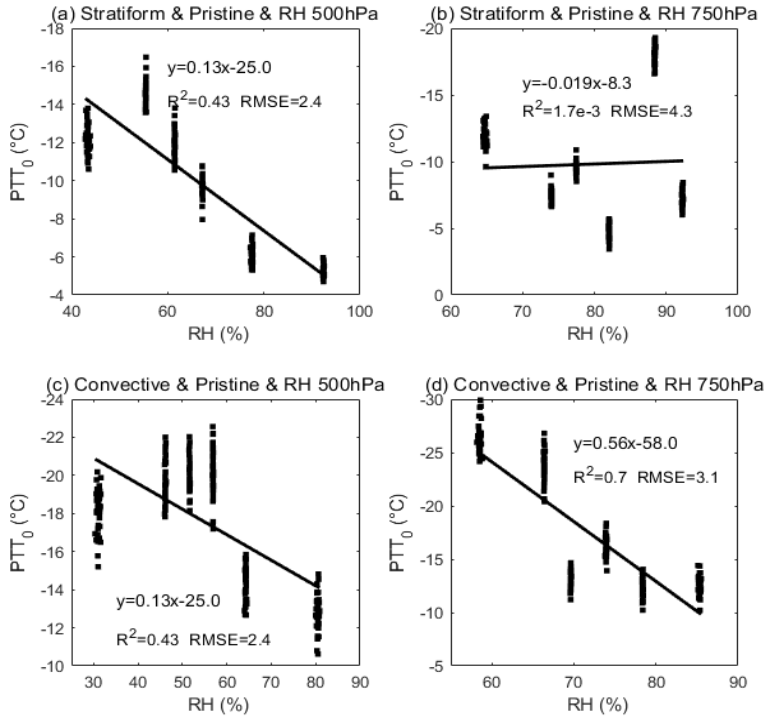

Figure S14: As same as Figure S12, but for relative humidity (RH, %) .